Separating natural and bomb-produced radiocarbon in the ocean: The potential alkalinity method

Stephany I. Rubin[1]
Lamont-Doherty Earth Observatory of Columbia University, Palisades, New York, USA

Robert M. Key
Atmospheric and Oceanic Sciences Program, Princeton University, Princeton, New Jersey, USA

Received 2 May 2001; revised 8 May 2002; accepted 9 September 2002; published 3 December 2002.

[1] The use of radiocarbon ($\Delta^{14}C$) as a tracer for oceanic processes generally requires differentiation of naturally occurring radiocarbon from the bomb component produced by atmospheric nuclear weapons testing. We present a new separation method based on the strong linear correlation between $\Delta^{14}C$ and potential alkalinity. Unlike previous techniques the new algorithm is applicable at all latitudes. Additionally, the potential alkalinity method provides an estimate of surface ocean prebomb $\Delta^{14}C$ concentrations. Predictions with the technique appear to be unbiased and have uncertainties which are less than previous techniques. *INDEX TERMS:* 4860 Oceanography: Biological and Chemical: Radioactivity and radioisotopes; 4894 Oceanography: Biological and Chemical: Instruments and techniques; *KEYWORDS:* bomb-produced radiocarbon, natural radiocarbon, radiocarbon separation, potential alkalinity method, silicate method, radiocarbon inventory

Citation: Rubin, S. I., and R. M. Key, Separating natural and bomb-produced radiocarbon in the ocean: The potential alkalinity method, *Global Biogeochem. Cycles*, *16*(4), 1105, doi:10.1029/2001GB001432, 2002.

1. Introduction

[2] For almost 50 years radiocarbon has been used as a tracer to study mixing processes and ventilation in the upper ocean, and as a proxy for anthropogenic CO_2 concentration. Both the power and the difficulty in using radiocarbon to study upper ocean processes stem from the atmospheric time-history. Interpretation is complicated by the fact that few oceanic measurements were made prior to surface water contamination by bomb-produced $\Delta^{14}C$.

[3] *Broecker et al.* [1985, 1995] proposed two methods to separate natural and bomb-produced $\Delta^{14}C$. In the first, the tritium method, measured prebomb surface $\Delta^{14}C$ values are directly linked to measured $\Delta^{14}C$ values at the depth where the tritium (^3H) concentration approaches zero. In the region between the ocean surface and the zero tritium depth, radiocarbon in excess of the estimated prebomb value is assumed to be bomb-produced. This method assumes that tritium and radiocarbon are transferred from the atmosphere to the ocean on a similar time scale and that they penetrate into the ocean in a similar manner, or that failure of either assumption has negligible influence. The method defines the near surface prebomb radiocarbon profile as a straight line. The first assumption is clearly violated since the transfer time for tritium is shorter than for radiocarbon and the transfer pathways are significantly different both chemically and physically.

[4] The second method used by *Broecker et al.* [1995], hereafter designated B95, relied on the correlation between dissolved silicate and $\Delta^{14}C$. This method provided an estimate of the shape of the prebomb radiocarbon profile (except for surface ocean values) and was found to be applicable for much of the global ocean. This is the currently accepted separation method and is examined in detail below.

[5] We present an alternative separation method based on the correlation between potential alkalinity (see definition below) and radiocarbon. This new algorithm is based on the same arguments provided in B95. The new method overcomes the spatial limitations of the silicate method, has lower error estimates, and produces estimates of surface ocean prebomb $\Delta^{14}C$.

[6] Both the silicate and potential alkalinity methods are based on circumstantial evidence. In the end the algorithms are empirical even though based on reasonable assumptions. In spite of this, we believe the effort worthwhile since there are currently no better alternatives.

[7] Our goal is to produce a simple, globally applicable function for predicting prebomb oceanic $\Delta^{14}C$ values. Statistical details are given where appropriate to the goal. In the following sections, we (1) describe the data set, (2) review the B95 silicate method, (3) describe

[1]Now at Department of Earth and Atmospheric Sciences, Georgia Institute of Technology, Atlanta, Georgia, USA.

0886-6236/02/2001GB001432$12.00

Table 1. Interpolation Limits

Depth Zone	$\Delta^{14}C$ Depth Range, m	Maximum Allowable Value Separation, m
1	0–200.999	100
2	201–750.999	200
3	751–1500.999	250
4	1501–10000	500

the potential alkalinity method, (4) compare results from the alkalinity method to those from the silicate and one other method, (5) describe calibration of the alkalinity method for prediction of surface ocean prebomb $\Delta^{14}C$ values, and (6) calculate inventories using the new method.

2. Data Set

[8] The analyses presented here are intentionally restricted to the GEOSECS data set as distributed on magnetic tape by the Physical and Chemical Ocean Data Facility (now WOCE-WHP) at Scripps Institution of Oceanography. Radiocarbon samples which were acquired by pumping rather than from Gerard barrels (listed in the GEOSECS shorebased analysis atlas [*Östlund et al.*, 1987]) were also included. The corrections suggested by *Craig et al.* [1981,

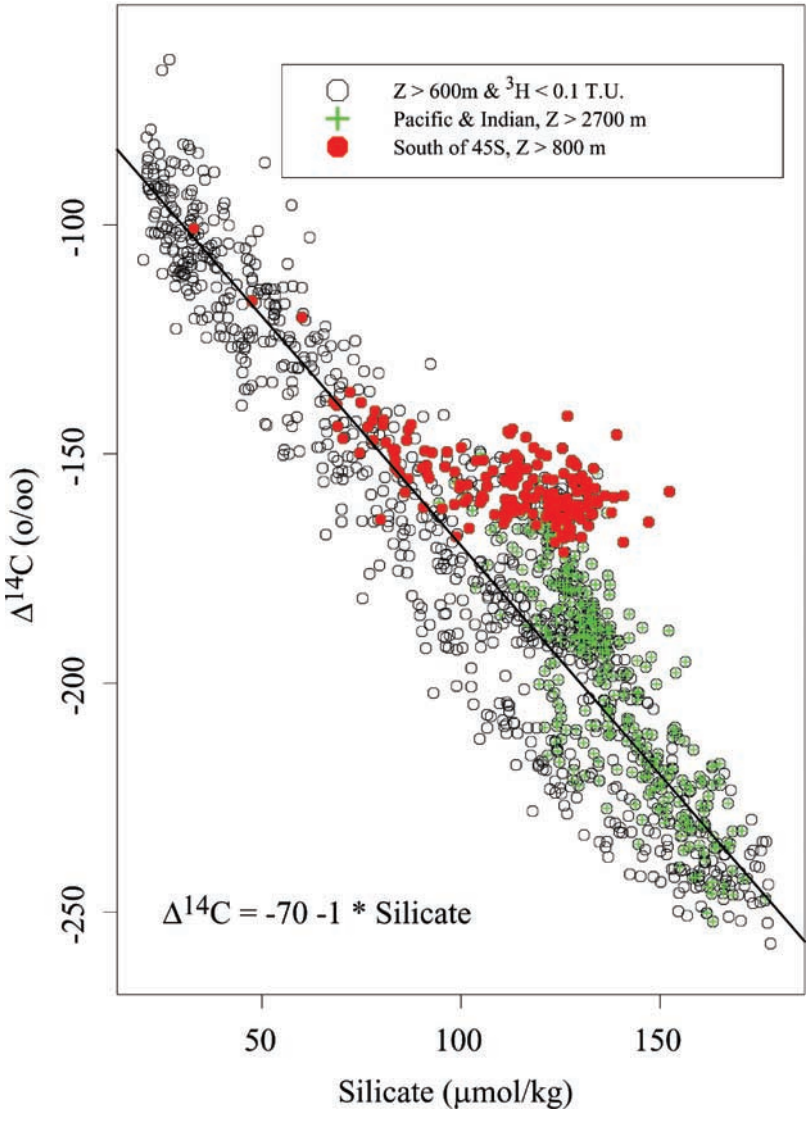

Figure 1. $\Delta^{14}C$-silicate correlation for deep (Z > 600 m), tritium free (H^3 < 0.1 TU) waters, measured during the GEOSECS program (open circles). Points overprinted with a green plus sign are the subset from the Indian and Pacific Oceans at depths greater than 2700 m. Points overprinted with red fill are the subset from latitudes south of 45°S and deeper than 800 m. The line is from B95, derived using approximately the data set shown except for the high southern latitude data. See Table 4 for statistical details.

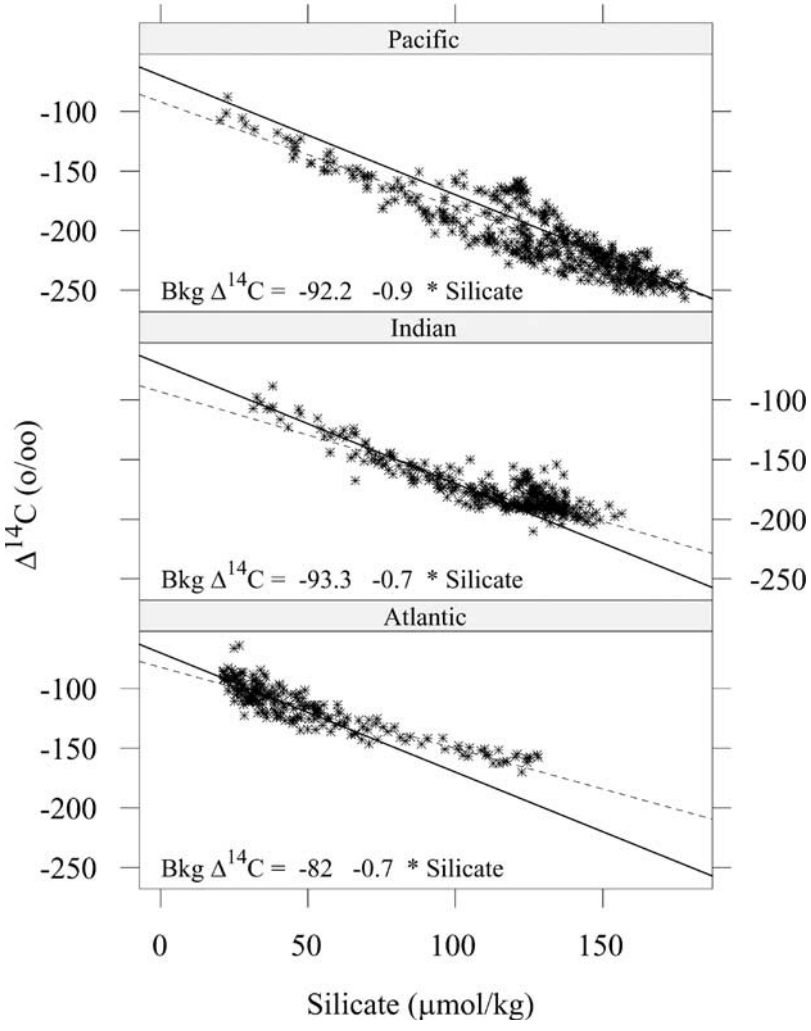

Figure 2. Data from Figure 1, excluding high southern latitude results, segregated by ocean. Each panel has the regression line from Figure 1 (thick solid line). The thin dashed lines are the fit for the data in each panel. The anomalous Indian Ocean points (silicate $\sim$ 125, $\Delta^{14}C \sim -175$) are from the deep Arabian Sea and Bay of Bengal (see text). See Table 4 for statistical details.

p. 2] were applied to the Pacific Ocean alkalinity measurements. The hydrographic data, alkalinity, tritium and radiocarbon values were subjected to quality control procedures that have become standard during the World Ocean Circulation Experiment [*Joyce and Corry*, 1994a, 1994b].

[9] Finally, since alkalinity and tritium were frequently not measured on the same sample bottles used for radiocarbon, values were interpolated to the radiocarbon locations using measured values (which had been judged "good" during the QC procedure) at the same station. The interpolation algorithm was a one-dimensional quasi-cubic Hermitian polynomial (IQHSCU from the IMSL, 1978 library). The maximum allowable data separation between which interpolation was performed increased with depth as summarized in Table 1. For example, if a $\Delta^{14}C$ measurement existed in Zone 1 and did not have an accompanying alkalinity, then an alkalinity value was interpolated if and only if alkalinity was measured at that station, good alkalinity values existed both above and below the $\Delta^{14}C$ measurement depth and the closest surrounding alkalinity values were no more than 100 m apart. Extrapolation was disallowed. This procedure resulted in 1194 samples with both $\Delta^{14}C$ and silicate and 1088 samples with both $\Delta^{14}C$ and potential alkalinity.

3. Silicate Method

[10] B95 introduced a method to separate natural and bomb-produced radiocarbon based on the linear relationship between natural $\Delta^{14}C$ and silicate (equation (1) where silicate is in μmole/kg and $\Delta^{14}C$ is in parts per thousand (‰ or permil)). This method assumes that the correlation found in the lower thermocline and deeper waters holds for the upper thermocline.

$$\text{Natural } \Delta^{14}C = -70 - \text{Silicate} \quad (1)$$

[11] Bomb-$\Delta^{14}C$ is then just the measured $\Delta^{14}C$ value less the natural component. B95 published figures and tables

Table 2. Summary Statistics for Silicate and Potential Alkalinity Regression Lines

Fit	Figure	Region	b_0[a]	b_1[b]	r^2[c]	σ[d]	n[e]	SSR[f]	SSE[g]	F[h]
Silicate[i]	Figure 1	All	−73.7 ± 1.3	−0.96 ± 0.01	0.88	15.0	999	1674771	224902	7424
	Figure 2	Atlantic[j]	−82.0 ± 1.2	−0.68 ± 0.02	0.82	9.0	216	76336	17155	952
	Figure 2	Pacific[k]	−92.2 ± 2.7	−0.88 ± 0.02	0.80	14.3	457	372870	92802	1828
	Figure 2	Indian[l]	−93.3 ± 2.4	−0.72 ± 0.02	0.80	9.6	326	115780	29733	1262
Palk[m]	Figure 3	All[m]	−59.0 ± 1.0	−0.962 ± 0.008	0.93	11.6	1084	1895485	145588	14140
	Figure 4	Atlantic[n]	−53.6 ± 1.6	1.00 ± 0.02	0.88	9.1	279	174132	23211	2078
	Figure 4	Pacific[o]	−52.6 ± 2.1	1.03 ± .01	0.92	10.2	436	538688	44746	5225
	Figure 4	Indian[p]	−97.4 ± 1.9	−0.63 ± 0.02	0.82	8.9	373	132546	29681	1657
Palk[q]	Figure 3	All[q]	−55.3 ± 0.9	−1.013 ± 0.007	0.95	9.8	944	1890205	91348	19490
	Figure 4	Indian[r]	−75.8 ± 2.6	−0.85 ± 0.02	0.83	8.2	229	72548	15266	1079

[a] Regression intercept with 1 standard error (‰Δ^{14}C).
[b] Regression slope with 1 standard error (‰Δ^{14}C/μmol kg^{-1} silicate).
[c] Coefficient of determination. This value can be interpreted as the proportionate reduction of total variation associated with the use of the independent variable.
[d] Residual standard error from fit (‰Δ^{14}C); $\sigma = \sqrt{SSE/(n-2)}$.
[e] Number of data points used in regression.
[f] Regression sum of squares from fit.
[g] Error sum of squares from fit.
[h] F-statistic for the fit with 1 and n−2 degrees of freedom. Given the size of n, these F values are all "huge." Stated alternately, for any of these regressions a test of linearity will pass and a test of equivalence between any two regressions will fail for any reasonable confidence level.
[i] Attempt to recreate the fit derived in B95 ($b_0 = -70$, $b_1 = -1$). Data included in Figure 1. Data restricted to: Depth > 600 m, 20 ≤ silicate(μmol/kg) ≤ 180, ^{3}H ≤ 0.1 TU; latitudes equator ward of 45°N/S.
[j] Bottom panel of Figure 2.
[k] Top panel of Figure 2.
[l] Center panel of Figure 2.
[m] Solid line and all data shown in Figure 3. The coefficients used here are those used in equation (3). Data restricted to: Depth > 600 m, 2300 ≤ potential alkalinity ≤ 2600, and ^{3}H ≤ 0.1 TU.
[n] Bottom panel Figure 4.
[o] Top panel Figure 4.
[p] Center panel and solid line Figure 4.
[q] Dashed line in Figure 3. This fit excludes anomalous deep North Indian Ocean points (Palk > 2450).
[r] Center panel Figure 4, dashed line. This fit excludes the anomalous deep North Indian Ocean points (Palk > 2450).

showing global surface values and inventories of bomb Δ^{14}C based on GEOSECS measurements. They investigated the transient nature of the bomb signal by comparing GEOSECS (1972–1973) results to TTO (Transient Tracers in the Ocean program; 1980–1981) results in the North Atlantic and SAVE (South Atlantic Ventilation Experiment, 1987–1989) results in the South Atlantic.

[12] The natural Δ^{14}C-silicate correlation is rather good for most ocean waters, because the distribution of each is controlled by the interaction of large scale circulation and

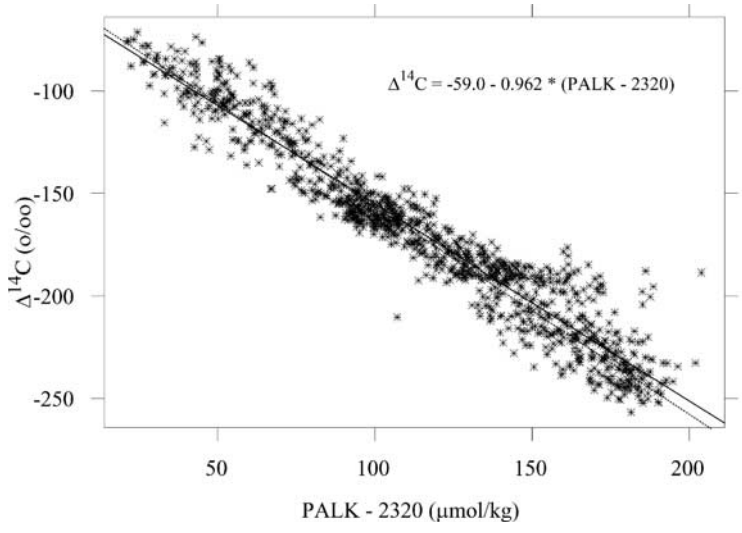

Figure 3. Radiocarbon data set from Figure 1 plotted as a function of potential alkalinity and left-shifted by the mean global surface potential alkalinity (2320). The regression equation and statistics for the least squares line are given (note d.f. = degrees of freedom; 1 standard deviation given for coefficients; see Table 4 for details). The dashed line shows the fit if the abyssal North Indian Ocean data points are excluded (see text).

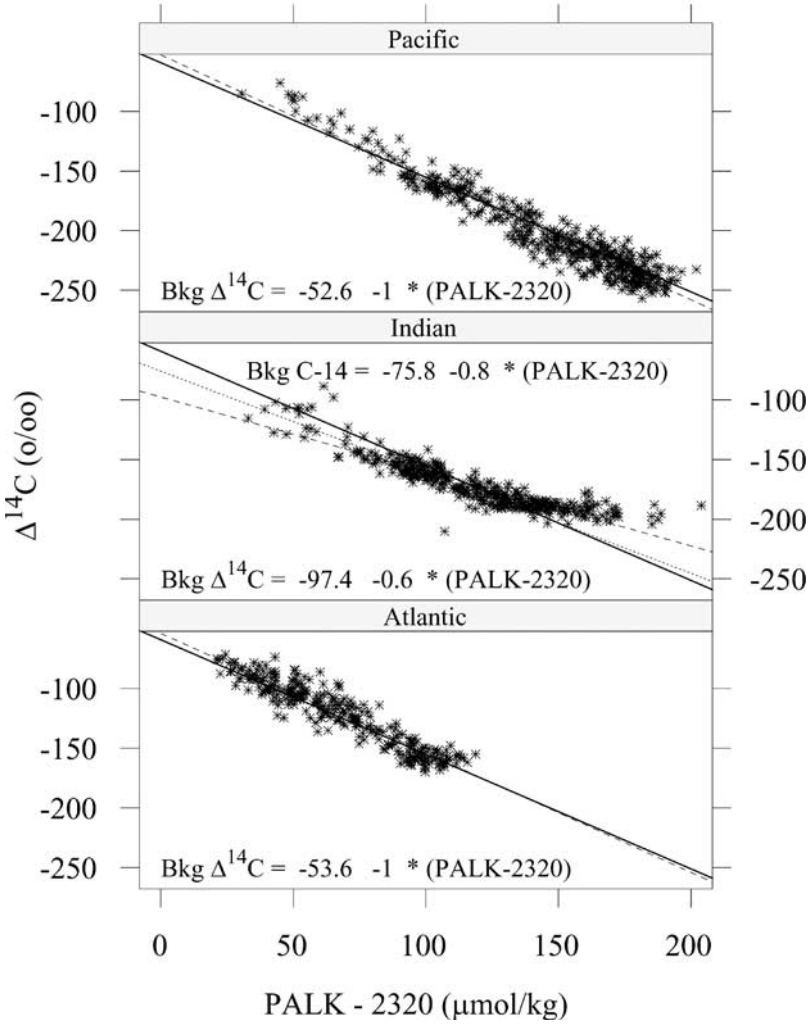

Figure 4. Data from Figure 3 segregated by ocean and individually fit by simple linear regression (dashed line). The anomalous high values in the Indian Ocean are all from the deep waters of the Bay of Bengal and Arabian Sea. The solid line is the same in each panel and is the global fit from Figure 3 and equation (3). If the anomalous data points from the deep northern Indian Ocean are excluded, the intercept and slope for the remaining points become −75.8 and −0.85, respectively. See Table 4 for statistical details.

biology. That is (1) both silicate and radiocarbon have oceanic residence times which are reasonably long relative to thermohaline circulation timescales, (2) both are biologically removed from surface waters and remineralized at depth in the water column, and (3) a significant fraction of each that does reach the seafloor redissolves into bottom waters.

[13] Referring to their Figure 1, B95 state that [*Broecker et al.*, 1995], "for tritium-free waters from greater than 1000 m collected during the GEOSECS survey, the points fall largely within 20‰" of the line defined by equation (1). They further note that for tritium-free thermocline waters from the major ocean basins (their Figure 2) [*Broecker et al.*, 1995], "the points lie almost entirely within ±10‰ of the same line." The data set used for the latter is much smaller than that used for the former. They state that circumpolar deep waters in the Antarctic are a major exception to the fit and that for the thermocline samples from the Atlantic north of 15°N a better fit is obtained with an intercept of −60 rather than −70. B95 do not state what data were used to define equation (1) nor do they give uncertainties for the coefficients or fit.

[14] In Figure 1 we have attempted to reproduce the B95 Figure 1 in order to define the data set used to find equation (1) and to approximate the uncertainties. Details of the data set used and regression results are given in Table 2. We were not able to exactly reproduce their coefficients, however, the derived uncertainty (±15‰) is a reasonable estimate and is comparable in scope (number of data points) to estimates derived below for the potential alkalinity method.

[15] Figure 2 shows the same data as Figure 1 except that the Southern Ocean data have been excluded and the data are segregated by ocean. Each panel includes the regression line from Figure 1 (solid line) and a second regression line which is the fit for the points in that panel (equation shown, dashed line). Details for the panel regressions are listed in

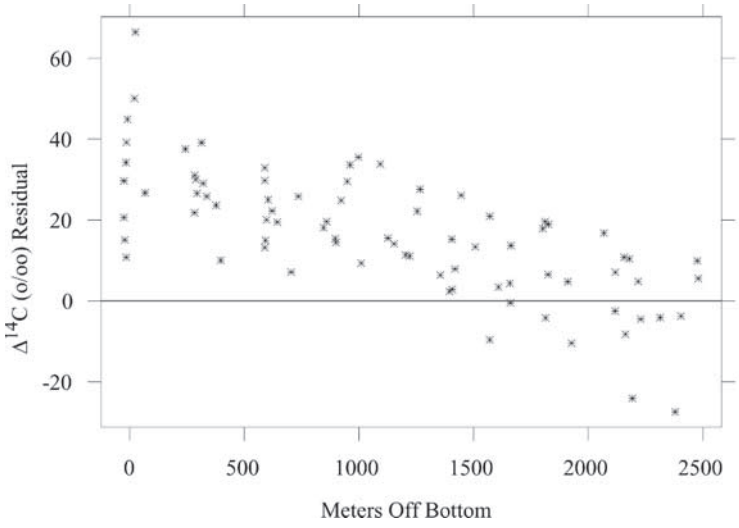

Figure 5. Residuals from the northern Indian Ocean data fit of radiocarbon versus potential alkalinity. The pattern of increasing residuals near the seafloor implies that dissolution of carbonate which has been contaminated by bomb-radiocarbon may be the cause.

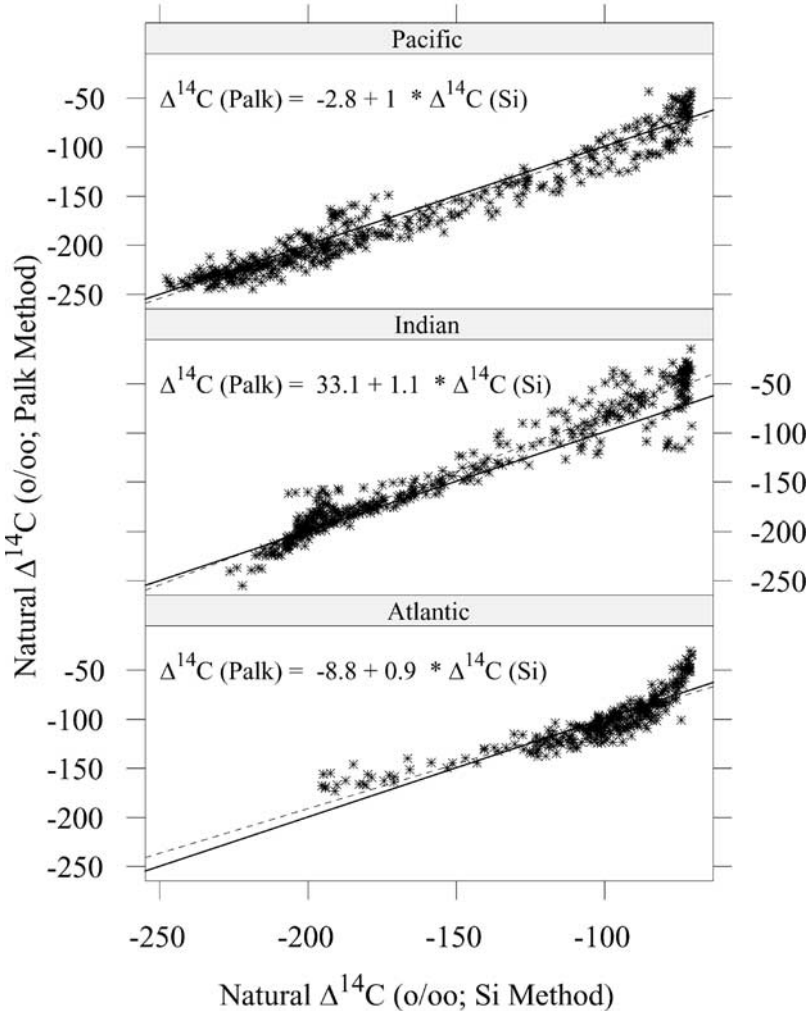

Figure 6. Comparison of natural Δ^{14}C using the Palk and silicate methods. With the exception of the youngest Atlantic waters, the results are remarkably similar.

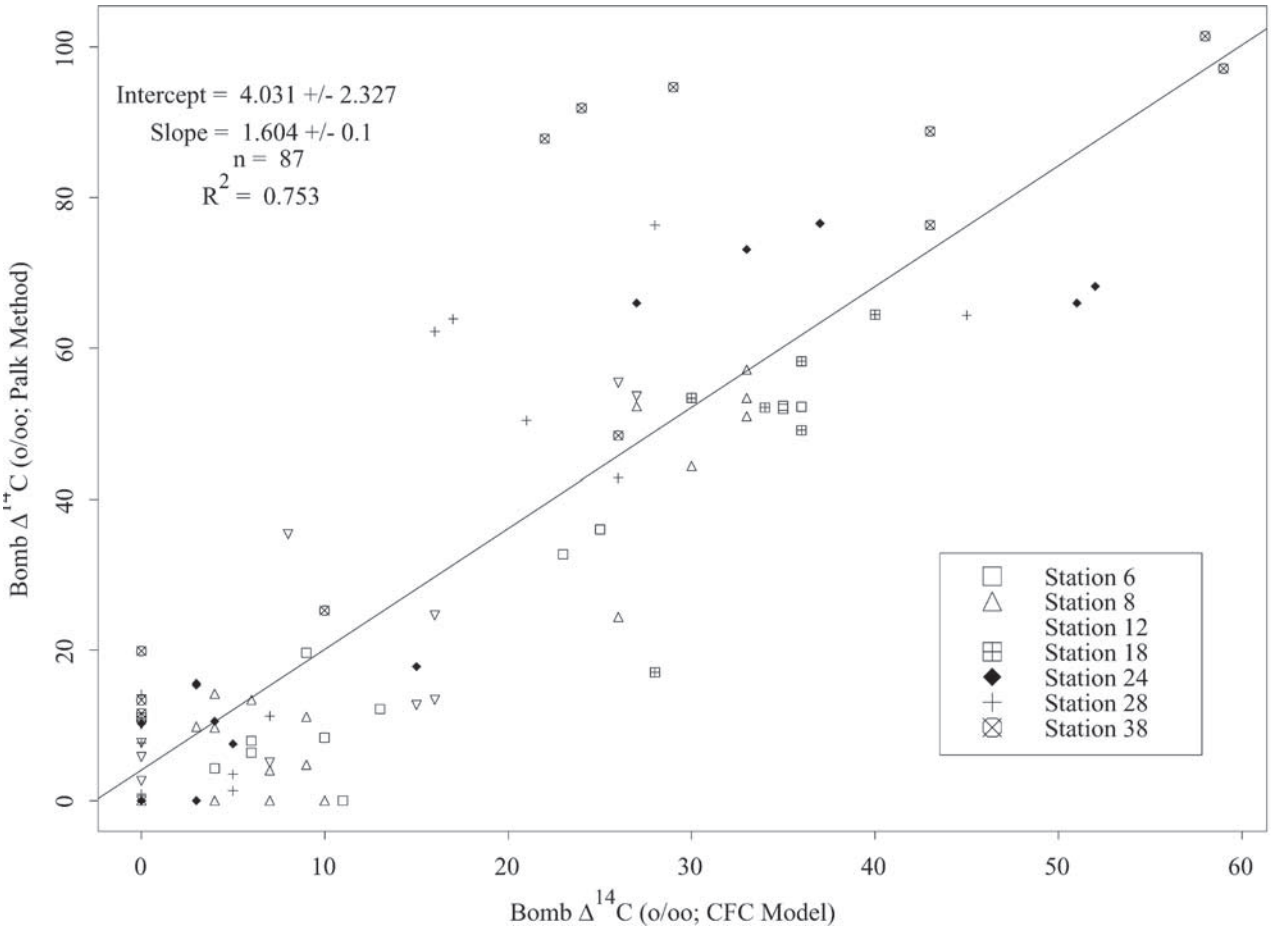

Figure 7. Comparison between predicted bomb $\Delta^{14}C$ using the Palk and CFC methods. Significant scatter exists, but the Palk method predicts values 1.6 times the CFC method. Presumably the difference is due to unaccounted for mixing with the CFC method.

Table 2. Also evident in Figure 1 and/or Figure 2 (and much more apparent in residual plots not included here), but not noted by B95 are that (1) the thermocline data and deep ocean data form two groupings each with visibly different slope and intercept, (2) the thermocline points have a concave down shape rather than a straight line, and (3) the ''by ocean'' regression coefficients differ substantially from the B95 values. Significant effort was expended trying to find a ''fix'' for these problems, however no acceptable improvement was discovered.

4. Potential Alkalinity Method

[16] When no satisfactory improvement was found for the silicate method, an alternate covariable was sought. We found that potential alkalinity (Palk, as defined by *Brewer and Goldman* [1976], but ignoring the minor phosphate correction) correlated highly with radiocarbon. Palk is essentially the alkalinity corrected for biological activity and normalized to salinity (equation (2)). The factors listed above which result in a near-linear silicate-radiocarbon relationship also influence the potential alkalinity-radiocarbon relationship. An improved relationship is not surprising since $CaCO_3$ carries both alkalinity and radiocarbon to depth. As $CaCO_3$ dissolves, alkalinity and radiocarbon are released with the $\Delta^{14}C$ signature of the water in which the carbonate formed. Because the ocean mixing time is much greater than the bomb radiocarbon input time history, the $\Delta^{14}C$ of deep water is relatively unaffected by the surface bomb component.

[17] Figure 3 shows the scatter plot and regression statistics (equation (3)) for $\Delta^{14}C$ versus potential alkalinity using the same GEOSECS data as in Figure 1 (depth > 600 m and $^3H < 0.1$ T.U.). This regression includes the high latitude data which was excluded from the silicate regression.

$$\text{Palk} = (\text{Alkalinity} + \text{Nitrate}) * 35/\text{Salinity} \quad (2)$$

$$\text{Natural } \Delta^{14}C = -59.0 - 0.962(\text{Palk} - 2320) \quad (3)$$

[18] The factor of 2320 included in equation (3) is the average global surface ocean potential alkalinity. This value, subsequently referred to as $Palk_0$, could have been incorporated into the intercept term. Equation (3) is written as it is to emphasize that $Palk_0$ is nothing more than a calibration factor that allows equation (3) to reasonably predict surface ocean natural $\Delta^{14}C$. Figure 4 is analogous to Figure 2. The anomalous Indian Ocean data were collected north of the equator at depths below ~2500 m. If these data are

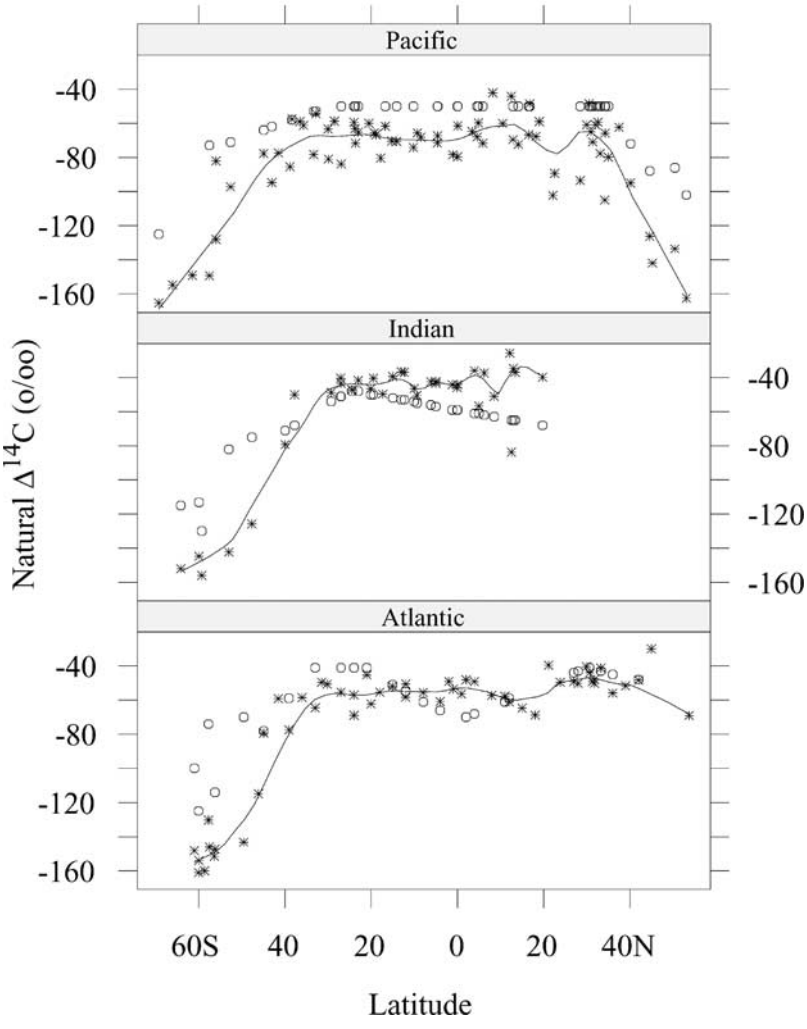

Figure 8. Predicted surface ocean natural $\Delta^{14}C$ (asterisks) using the Palk method segregated by ocean and plotted against latitude. Also shown are the values from B95 (circles).

excluded from the global regression, then the intercept, slope, r^2, and residual standard error become, respectively, -55.3 ± 0.9, -1.013 ± 0.007, 0.95, and 9.8 based on 944 remaining measurements.

[19] The anomalous measurements occur in both the Arabian Sea and Bay of Bengal. The points fall above the global trend indicating that either Palk or $\Delta^{14}C$ is high. This in turn implies either anomalously high alkalinity and/or nitrate in the deep water relative to the global average or an additional radiocarbon source.

[20] The Bay of Bengal (BB) and particularly the Arabian Sea (AS) are well documented sites of high biological activity. The flux of particulate carbonate has been reported to be approximately the same in both areas (BB = 10.72–16.08 g m^{-2} yr^{-1}, *Ittekkot et al.* [1991]; AS = 11.88–16.08 g m^{-2} yr^{-1}, *Nair et al.* [1989]), however recent results from the Joint Global Ocean Flux Study (JGOFS) in the open AS are lower (annual mean organic carbon = 1.3 g m^{-2} yr^{-1}; inorganic carbon = 1.7 g m^{-2} yr^{-1}; *Honjo et al.* [1999]). *George et al.* [1994] gave a detailed report of the premonsoon carbon chemistry of this region. They found a south to north TCO_2 increase of 50 μmole/kg in the deep AS. Approximately half this increase was attributed to dissolution of carbonate particles and the other half to remineralization of organic carbon. In the BB the south to north TCO_2 increase was only ~40% of that in the AS and of this increase only about 15% was due to organic carbon remineralization.

[21] One possible cause for the anomalous residuals in the deep northern Indian Ocean is transport of bomb radiocarbon from the surface ocean to the sediments in carbonate particles followed by dissolution and subsequent mixing back up into the water column. This process occurs over most of the ocean, however, in most areas the bomb radiocarbon added to deep water by dissolution of carbonate at the sea-floor is small relative to the affects of decay and circulation [*Fiadiero*, 1982]. If this hypothesis is correct, one might reasonably expect to see the residuals in the northern Indian Ocean decrease with height off the bottom. This is indeed the case. Figure 5 shows that the residuals from the global potential alkalinity fit for the northern Indian Ocean decrease away from the seafloor. If this explanation is accepted, then the conclusion follows that

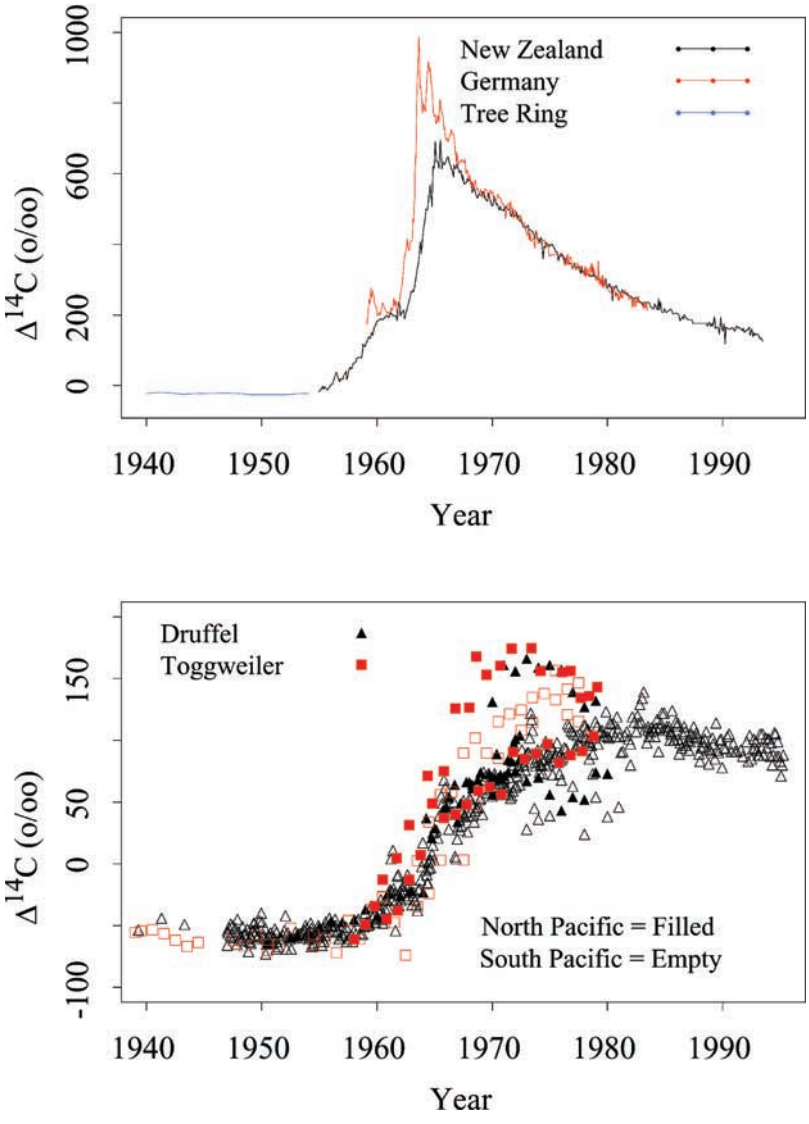

Figure 9. (top) Atmospheric time history of Δ^{14}C. The difference between values measured in Germany [*Levin et al.*, 1995] and New Zealand [*Manning and Melhuish*, 1994] is because most atmospheric nuclear tests were carried out in the Northern Hemisphere. Tree ring data are from *Stuiver et al.* [1998]. (bottom) Pacific Ocean surface values for Δ^{14}C. The trends are similar to those in the atmosphere. Data are from coral measurements [*Druffel*, 1981, 1987; *Toggweiler et al.*, 1991].

the bottom waters of the BB and AS have measurable bomb ^{14}C contamination. Recent work by *Sabine et al.* [2002] indicates that carbonate dissolution in the northern Indian Ocean occurs at shallower depths and to a greater degree than previously thought.

5. Method Comparison

[22] The regression fit for the potential alkalinity method ($r^2 = 0.93$; $\sigma = 12$) is better than for the silicate method ($r^2 = 0.88$; $\sigma = 15$). If the deep northern Indian Ocean measurements are excluded from the potential alkalinity fit, then the difference is greater ($r^2 = 0.95$; $\sigma = 10$). More importantly, the potential alkalinity method can be used for all latitudes and, as will be shown later, can be used to predict prebomb surface ocean Δ^{14}C values.

[23] Figure 6 shows the relationship between the predicted natural Δ^{14}C values using the Palk method and the silicate method plotted by ocean. The data shown in the figure were limited to samples from latitudes between 40°S and 40°N. For the regression, the additional limitation of measured Δ^{14}C less than −75‰ was imposed. The latitude restriction limits the data to the approximate data range specified by B95. The radiocarbon limit excludes very near surface values where silicate concentrations approach zero and where seasonal factors could be important. With these restrictions, and considering the measurement errors, the two techniques produce similar estimates. In each sub panel

Table 3. Early Radiocarbon Measurements and Estimated Value Prior to Contamination

Lat.	Long.	Sample Time	Ocean	Meas. $\Delta^{14}C$‰	Corr. $\Delta^{14}C$‰	Palk	$Palk_0$	Ref.
−15.200	−179.100	1958.250	S. Pac.	−41	−43.4	2306	2317	1[a]
−18.300	−172.300	1958.250	S. Pac.	−43	−45.4	2302	2312	1
−20.900	−175.400	1958.250	S. Pac.	−36	−38.4	2295	2312	1
−21.300	−177.500	1958.250	S. Pac.	−40	−42.4	2297	2310	1
−21.300	173.300	1958.250	S. Pac.	−38	−40.4	2297	2312	1
−28.800	176.000	1958.250	S. Pac.	−42	−44.4	2300	2310	1
−32.900	175.800	1958.250	S. Pac.	−43	−45.4	2299	2309	1
−36.600	174.900	1958.250	S. Pac.	−50	−52.4	2314	2315	1
−37.400	170.600	1958.250	S. Pac.	−58	−60.4	2316	2310	1
−41.100	178.000	1956.583	S. Pac.	−47	−50.1	2326	2338	1
−46.200	171.200	1958.167	S. Pac.	−63	−65.0	2342	2331	1
−51.500	169.100	1958.167	S. Pac.	−70	−72.0	2338	2320	1
−59.900	169.600	1958.167	S. Pac.	−91	−93.0	2395	2355	1
−66.500	164.000	1958.167	S. Pac.	−128	−130.0	2395	2316	1
−34.800	−135.900	1957.917	S. Pac.	−38	−38.9	2307	2324	2[b]
−42.700	−96.000	1958.000	S. Pac.	−40	−41.2	2331	2345	2
−46.500	−116.000	1958.000	S. Pac.	−60	−61.2	2342	2336	2
19.583	−125.0000	1958.917	N. Pac.	−40	−51.6	2302	2309	2
5.000	−130.0000	1958.917	N. Pac.	−40	−51.6	2298	2305	2
−7.000	−132.000	1958.917	S. Pac.	−42	−49.6	2296	2302	2
−34.833	−135.883	1958.917	S. Pac.	−38	−45.6	2307	2318	2
−46.500	−116.000	1958.917	S. Pac.	−60	−67.6	2342	2330	2
−42.717	−96.000	1958.917	S. Pac.	−62	−69.6	2331	2316	2
62.600	−8.000	1957.250	N. Atl.	−41	−43.07	2330	2341	3[c]
67.800	−25.100	1957.333	N. Atl.	−67	−69.3	2327	2311	3
65.500	−26.600	1957.333	N. Atl.	−53	−55.3	2327	2326	3
64.800	−35.500	1957.333	N. Atl.	−43	−45.3	2328	2337	3
72.900	41.800	1957.583	N. Atl.	−45	−48.1	2325	2331	3
73.900	33.600	1957.583	N. Atl.	−40	−43.1	2325	2336	3
38.367	−71.533	1955.833	N. Atl.	−62	−61.5	2314	2308	4[d]
37.967	−50.883	1955.583	N. Atl.	−34	−33.5	2313	2337	4
36.100	−66.100	1955.917	N. Atl.	−52	−51.5	2306	2311	4
34.100	−65.100	1955.917	N. Atl.	−56	−55.5	2302	2302	4
34.083	−65.000	1957.917	N. Atl.	−54	−57.5	2302	2298	4
33.833	−66.300	1956.500	N. Atl.	−59	−59.2	2301	2296	4
33.000	−49.800	1956.500	N. Atl.	−58	−58.1	2300	2296	4
32.633	−57.917	1956.500	N. Atl.	−44	−44.2	2300	2310	4
31.750	−34.633	1956.500	N. Atl.	−65	−65.12	2298	2287	4
29.950	−61.683	1957.917	N. Atl.	−34	−37.5	2298	2314	4
29.217	−60.500	1957.917	N. Atl.	−33	−36.5	2298	2315	4
27.083	−73.533	1955.917	N. Atl.	−55	−54.5	2298	2299	4
25.700	−79.383	1957.500	N. Atl.	−44	−46.9	2298	2305	4
25.417	−75.217	1955.917	N. Atl.	−45	−44.5	2299	2310	4
20.533	−68.500	1955.917	N. Atl.	−44	−43.5	2301	2314	4
19.966	−70.883	1955.917	N. Atl.	−51	−50.5	2302	2307	4
19.117	−67.117	1955.917	N. Atl.	−46	−45.5	2302	2312	4
15.050	−39.800	1957.917	N. Atl.	−47	−50.5	2302	2305	4
19.067	−80.800	1956.000	N. Atl.	−57	−56.6	2302	2305	4
16.283	−79.233	1956.000	N. Atl.	−76	−75.6	2302	2281	4
17.650	−79.067	1956.000	N. Atl.	−53	−52.6	2302	2305	4
12.450	−77.417	1956.000	N. Atl.	−46	−45.6	2300	2311	4
17.083	−71.600	1955.917	N. Atl.	−52	−51.5	2302	2306	4
16.717	−70.633	1955.917	N. Atl.	−55	−54.5	2302	2303	4
17.183	−68.917	1955.917	N. Atl.	−61	−60.5	2302	2297	4
17.783	−68.367	1955.917	N. Atl.	−51	−50.5	2302	2308	4
34.067	26.350	1956.667	N. Atl.	−63	−63.5	2302	2292	4
0.850	−32.867	1958.000	N. Atl.	−76	−79.8	2300	2273	4
−3.100	−32.433	1956.167	S. Atl.	−55	−58.2	2299	2302	4
−3.567	−31.367	1956.167	S. Atl.	−61	−64.2	2298	2296	4
−4.483	−34.900	1957.083	S. Atl.	−73	−74.1	2298	2282	4
−5.683	10.650	1957.417	S. Atl.	−68	−68.1	2298	2286	4
−9.633	−34.083	1958.000	S. Atl.	−56	−57.2	2299	2297	4
−10.983	−32.467	1957.083	S. Atl.	−52	−53.1	2301	2307	4
−23.200	−37.633	1958.000	S. Atl.	−39	−40.2	2298	2313	4
−14.500	7.567	1957.417	S. Atl.	−58	−58.1	2304	2303	4
−25.517	12.433	1957.417	S. Atl.	−60	−60.1	2297	2294	4
−32.217	16.333	1957.333	S. Atl.	−51	−512	2297	2304	4
−34.100	18.100	1958.333	S. Atl.	−56	−59.0	2304	2299	4
−34.767	6.483	1957.333	S. Atl.	−42	−42.2	2307	2323	4
−39.050	−41.800	1957.333	S. Atl.	−54	−54.2	2321	2325	4
−40.900	−20.483	1957.333	S. Atl.	−58	−58.2	2326	2325	4

Table 3. (continued)

Lat.	Long.	Sample Time	Ocean	Meas. Δ^{14}C‰	Corr. Δ^{14}C‰	Palk	Palk$_0$	Ref.
−41.250	−6.167	1957.333	S. Atl.	−59	−59.2	2326	2325	4
−40.717	−56.533	1957.333	S. Atl.	−79	−79.2	2325	2303	4
−41.083	−51.150	1957.333	S. Atl.	−74	−74.2	2326	2309	4
−45.400	−59.217	1957.250	S. Atl.	−78	−78.4	2339	2319	4
−51.450	2.633	1958.250	S. Atl.	−88	−90.4	2338	2301	4
−55.4500	−57.167	1958.167	S. Atl.	−111	−113.0	2366	2305	4
−57.117	−7.250	1958.250	S. Atl.	−120	−122.4	2386	2315	4
5.533	−120.083	1959.583	N. Pac.	−79	−99.7	2298	2262	5[e]
30.067	−117.967	1959.750	N. Pac.	−13	−36.4	2298	2330	5
27.567	−59.633	1957.583	N. Atl.	−33	−36.1	2298	2316	5

[a] *Rafter* [1968].
[b] *Bien et al.* [1965].
[c] *Fonselius and Östlund* [1959].
[d] *Broecker et al.* [1960].
[e] *Bien et al.* [1960].

the solid line was derived for the global data set and the dashed line is for the ocean specific subset. Summary statistics for the global regression are given in equation (4). The results for the three oceans are remarkably similar with only the high Δ^{14}C values in the Atlantic being a bit anomalous relative to the global regression. B95 noted that for the North Atlantic north of 15°N a better fit for silicate was obtained if the intercept in equation (1) was changed from −70‰ to −60‰. This modification would move the anomalous points to the right and thus closer to a 1-to−1 relationship with the potential alkalinity estimate.

$$\Delta^{14}C_{Palk} = (1.5 \pm 1.3) + (1.0056 \pm 0.0081) * \Delta^{14}C_{Si} \quad (4)$$
$$R^2 = 0.93$$

Residual Standard Error = 14.4 on 1138 degrees of freedom

$$\text{Subset} = \Delta^{14}C < -75‰ \quad (5)$$

[24] *Leboucher et al.* [1999] developed an independent method, based on a simple model, for separating natural and bomb radiocarbon at high latitudes. The model is a variant one developed by *Jenkins* [1980] to study thermocline ventilation and is given by equation (6), where $C_{0,\ (t\ -\ \tau)}$ is the surface water concentration at time (t − τ), τ is the time lag required for a water parcel to travel from the surface to depth z, $C_{z,\ t}$, and $C_{z,\ t+1}$ are the concentrations at depth z in years t and t + 1, and η is the annual ventilation rate defined as the fraction of water at z replaced by water originating at the surface during the time step Δ*t*.

$$C_{z,t+1} = C_{z,t} + \eta\left[C_{0,(t-\tau)} - C_{z,t}\right] \quad (6)$$

[25] The model is calibrated using the atmospheric history and solubility of CFC-11 or CFC-12. This yields values for τ and η which are then used with the atmospheric Δ^{14}C history to determine the bomb component at z.

[26] *Leboucher et al.* [1999] did not compare bomb Δ^{14}C values generated with the silicate method to those generated with the CFC method, however, where possible, they did compare bomb Δ^{14}C inventories and reported varied results.

[27] Figure 7 shows a direct comparison of the bomb Δ^{14}C results from their Table 1 with values calculated using the Palk method. The station locations trend from south (Station 6 at 68°S) to north (Station 38 at 49.7°S). The correlation between these 2 techniques is not as good as between the Palk and silicate techniques (r^2 = 0.75). More interesting is the fact that the Palk method predicts bomb Δ^{14}C values which are 1.6 times larger than the CFC method, presumably because of unaccounted-for mixing in the CFC method.

6. Palk$_0$ Calibration

[28] Figure 8 shows the surface ocean natural Δ^{14}C values predicted with equation (3) plotted against latitude (asterisks). Also shown (circles) are the measured prebomb surface values interpolated to GEOSECS station locations from B95 (B95, Table 1). The results are similar between 40°N

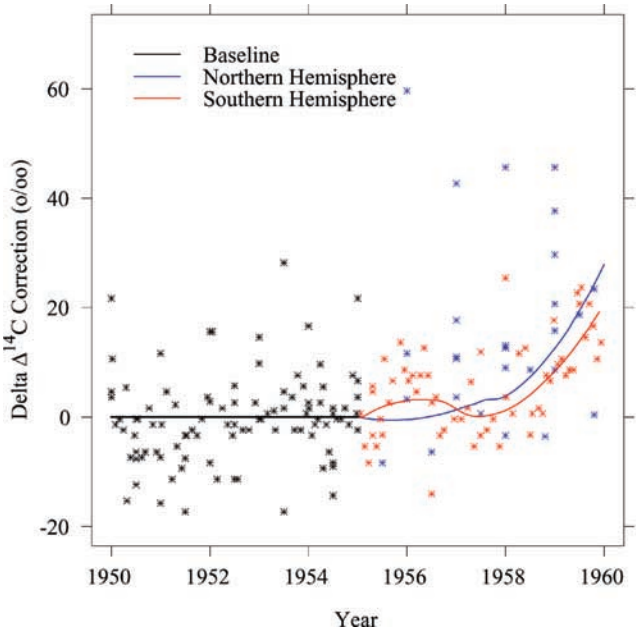

Figure 10. Lines indicate the estimated correction, derived from coral measurements, which was applied to the early surface ocean ^{14}C measurements. The uncertainty in the correction is about the same size as the correction itself; however, omitting this would lead to a systematic error rather than random error.

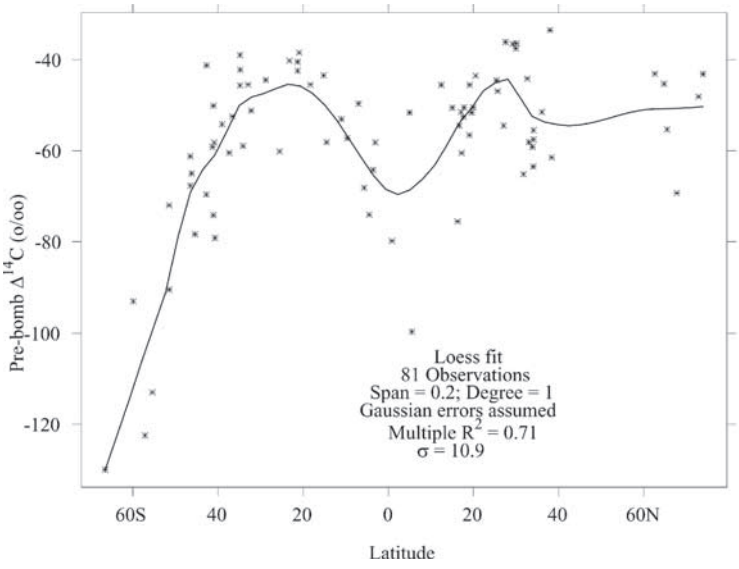

Figure 11. Early surface ocean $\Delta^{14}C$ measurements corrected to prebomb levels then fitted with a loess function. The error of the fit is approximately the same as the uncertainty in the individual data points.

and 40°S. In high latitudes, the Palk method predicts lower surface ocean natural $\Delta^{14}C$ values. The final step in development of the Palk method is to calibrate equation (3) so that it more reliably predicts surface values.

[29] The goal of the following is to replace the constant $Palk_0$ value (2320) in equation (3) with a simple function so that the equation accurately predicts prebomb surface ocean values. The derivation involves a number of steps, but each is rather simple: (1) Assemble the early surface ocean $\Delta^{14}C$ measurements and the best possible surface ocean potential alkalinity data set. (2) Assume that accumulation of bomb-produced radiocarbon in low latitude corals reflects the surface ocean radiocarbon history for the entire hemisphere (north or south) in which the coral grew. (3) Use the coral results to correct the early water measurements to the prebomb era. (4) Determine a simple relationship between the corrected early water measurements and the surface ocean potential alkalinity distribution for each hemisphere. (5) Replace $Palk_0$ in equation (3) with the derived function(s).

[30] The upper panel of Figure 9 shows the atmospheric $\Delta^{14}C$ level over the last 60 years. The Northern Hemisphere values are considerably higher than those in the Southern Hemisphere during the 1960s. The difference is due to two facts: (1) Most of the large atmospheric tests were carried out north of the equator. (2) There is a time lag in atmospheric transport across the equator.

[31] The lower portion of Figure 9 shows a similar trend measured in surface ocean water and coral samples from the Pacific Ocean; that is, a sharp increase in concentration in the early 1960s and a N-S hemispheric offset at the time of maximum concentration. The geographic distribution of early surface ocean $\Delta^{14}C$ measurements is sparse and not uniformly distributed. Very few vertical profiles were measured prior to the large atmospheric nuclear tests.

[32] The early $\Delta^{14}C$ measurements are listed in Table 3 and are essentially the same as those used in B95. In spite of following the B95 references back, we were unable to identify exactly what data sources they used. The data set was restricted to samples collected prior to 1960. This limits the available data, but also limits the potential error in the applied correction. Coral results were taken from *Toggweiler et al.* [1991], *Druffel* [1995], *Guilderson and Schrag* [1999], and *Guilderson et al.* [1999]. No trend was found in the merged coral data set for the period 1945–1955, so data from these years were averaged and used as the prebomb coral baseline (mean = −57.96‰, standard deviation = 6.7‰, standard error = 0.62‰, n = 116). The coral data from January 1956 through December 1959 were segregated by hemisphere and fitted with loess functions (Southern Hemisphere: span = 0.85, 3.8 equivalent parameters, $\sigma \sim 6.5$, n = 60; Northern Hemisphere: span = 0.85, 4 equivalent parameters, $\sigma = 13.5$, n = 37; errors assumed symmetric for both).

[33] To get the adjustment value for the early surface ocean measurements, the hemisphere-specific coral data fits were shifted by the baseline derived for 1945–1955. That is, the adjustment value is zero for January 1, 1956. Figure 10 summarizes the coral derived adjustment functions used to correct the early surface ocean radiocarbon measurements to prebomb levels. For 1956–1959 the adjustments for the surface ocean measurements range from 0–32‰ with an uncertainty of ~10‰. While the uncertainty in the adjustment is large relative to the magnitude of the adjustment, it is justified. The measurement error for the early data is approximately the same as the adjustment uncertainty. Additionally, failure to make this adjustment would result in a systematic bias of order 10‰ rather than a random error. The corrected surface ocean values are plotted against latitude in Figure 11 and listed in Table 3. Worth noting is that all of the high northern latitude data are from the Atlantic.

[34] The last step in the calibration procedure is to develop a functional relationship between the prebomb values shown in Figure 11 and surface ocean potential alkalinity. This procedure is a bit more complicated than it

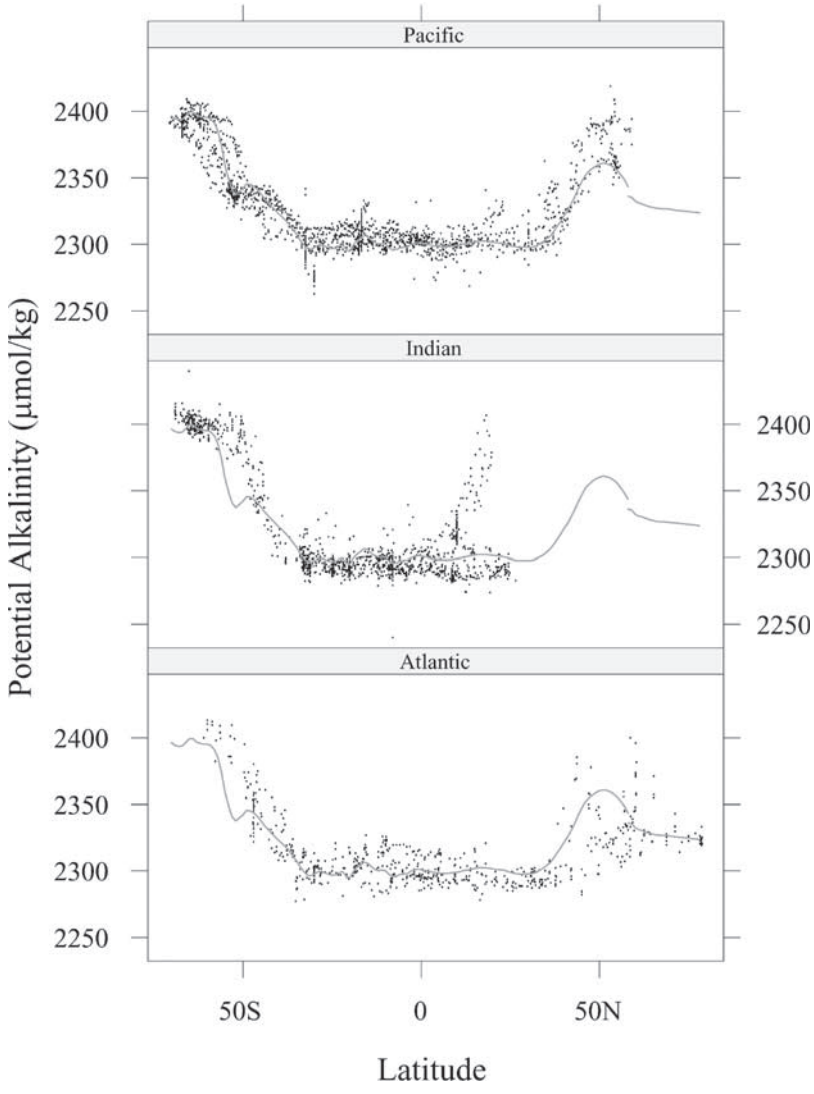

Figure 12. Surface ocean distribution of potential alkalinity. The smooth curve was derived using the combined global data and two loess functions joined at 58°N. The anomalous points in the northern Indian Ocean are from the Bay of Bengal.

might be because none of the early radiocarbon measurements were accompanied by sufficiently high quality (if any) alkalinity measurements. Therefore, potential alkalinity estimates must be made to accompany the radiocarbon data. The potential alkalinity approximation is derived using modern data and the steady state assumption.

[35] For the Indian and Pacific Oceans, surface ocean alkalinity, nitrate and salinity data were taken from WOCE cruises (as described by *Sabine et al.* [1999] and *Lamb et al.* [2002]). For the Atlantic Ocean, data from GEOSECS, TTO, SAVE and WOCE sections A20 and A22 were combined. For this compilation, the surface ocean was defined as 0–25 m. To get a satisfactory fit to the combined global surface ocean potential alkalinity, two loess fits were used with the division point occurring at 58°N. In calculating the fits, no attempt was made to weight the data by ocean area, so the Indian Ocean data may have influenced the result to a greater degree than justified. This potential bias is presumed to be much smaller than other unavoidable uncertainty. The derived function is summarized in Figure 12 with the data segregated by ocean. The global fit gives a good approximation except for the anomalously high points in the northern Indian Ocean (Bay of Bengal) and for the North Atlantic between latitudes 40°N and 55°N. If sufficient prebomb radiocarbon data become available to justify the complication, different fits could easily be derived for the individual oceans. The global fit is used to approximate potential alkalinity for each of the early radiocarbon measurements (Table 3).

[36] Equation (7) is the same as equation (3) rearranged with $Palk_0$ substituted for the constant value 2320. The corrected surface ocean radiocarbon values and the potential alkalinity values just derived are substituted into equation (7), $Palk_0$ values calculated (Table 3), and a simple functional form sought. Figure 13 shows the calculated $Palk_0$ values plotted against the absolute value of latitude for the radiocarbon data. A straight line was fit to the data for

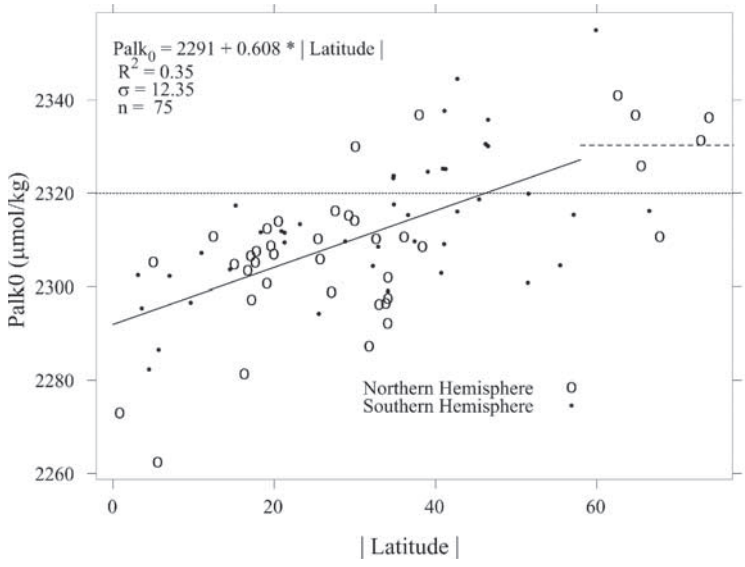

Figure 13. Calibration function used for $Palk_0$. The derived fits are not especially good, however, this calibration amounts to a minor adjustment to the original relationship given in equation (3).

latitudes south of 58°N. For latitudes north of 58°N (i.e., the far North Atlantic), the radiocarbon values were simply averaged (average = 2330, standard deviation = 11, standard error = 4.5, n = 6).

[37] The functions found for $Palk_0$ (equation (8)) are not particularly impressive, however, the uncertainty is similar to previously encountered errors. It should be remembered that this calibration procedure amounts to a relatively minor adjustment to the values which would have been directly derived from equation (3).

$$Palk_0 = \frac{(\Delta^{14}C + 59 + 0.962Palk)}{0.962} \tag{7}$$

$$Palk_0 = \begin{pmatrix} 2291 + 0.608|latitude| & \text{South of } 58°N \\ 2330 & \text{North of } 58°N \end{pmatrix} \tag{8}$$

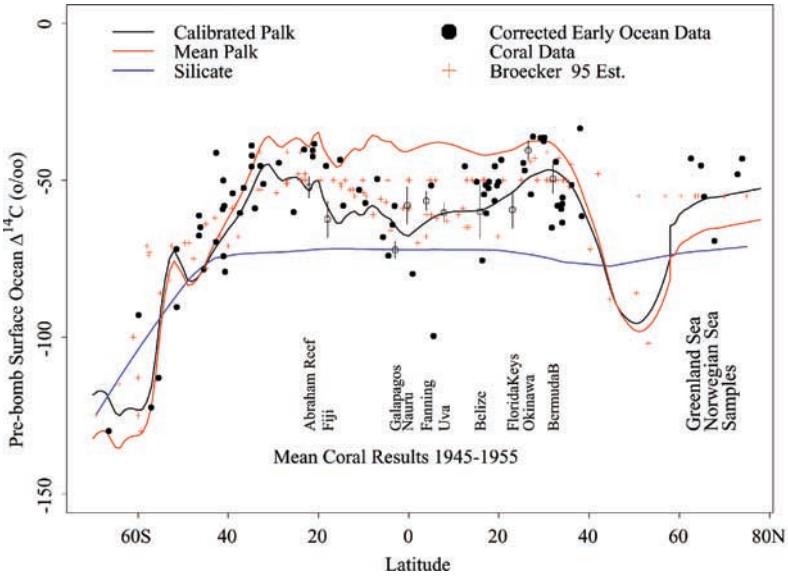

Figure 14. Estimates of the prebomb surface ocean $\Delta^{14}C$ distribution. The black, red and blue lines were generated using equations (9), (3), and (1), respectively, with either the surface ocean potential alkalinity from Figure 12 or the GEOSECS surface ocean silicate measurements (as appropriate). The black solid circles are the early surface ocean $\Delta^{14}C$ measurements corrected for bomb contamination (Table 2). The red pluses are the surface ocean prebomb $\Delta^{14}C$ estimates used by B95 for the GEOSECS stations. The open circles are the average coral values for the period 1945–1955 with 1 standard deviation error bars.

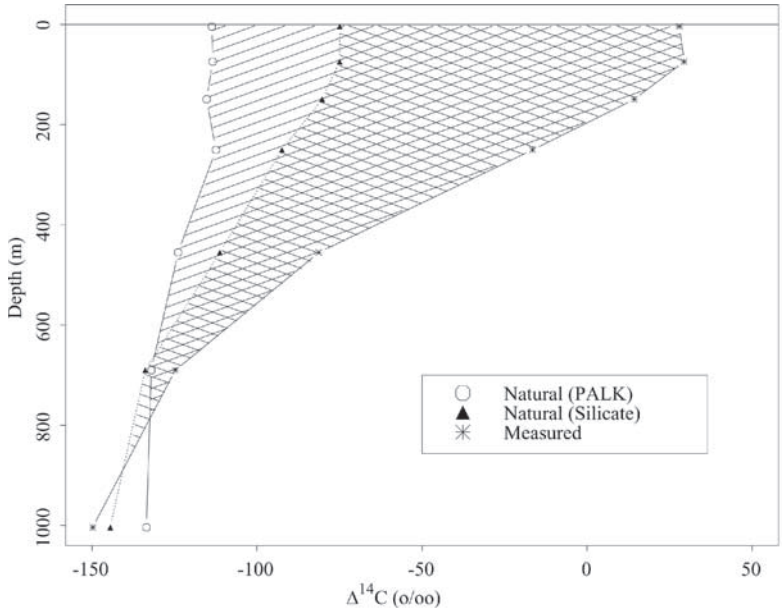

Figure 15. Measured $\Delta^{14}C$ results from GEOSECS Station 429 in the southern Indian Ocean along with estimated natural $\Delta^{14}C$ using both the potential alkalinity and silicate methods. The double hatched region indicates the bomb radiocarbon inventory using the silicate method. The potential alkalinity method adds the single hatched area to the inventory estimate.

$$\text{Natural } \Delta^{14}C = \left(\frac{59 + 0.962(\text{Palk} - 2291 - 0.608|\text{latitude}|}{59 + 0.962(\text{Palk} - 2330)\text{North of}58^{\circ}\text{N}}\right) \quad (9)$$

Finally, substituting equation (8) for the constant value of 2320 in equation (3) gives the calibrated prediction function for natural radiocarbon in surface waters.

[38] Figure 14 compares results using equation (9) with the alternatives. The black dots are the corrected surface ocean measurements made prior to 1960 (data from Figure 11), the red pluses are the surface ocean estimates (Table 4) used by B95 which were derived by interpolation from the uncorrected early surface ocean measurements, and the open circles with one standard deviation error bars are the mean results from 1945 to 1955 coral measurements. The labels below these points identify the coral locations. The black line was generated using equation (9) and the global fit to the surface ocean potential alkalinity shown in Figure 12. The red line was generated using the same potential alkalinity with the uncalibrated potential alkalinity function (equation (3)). Comparison of these two lines shows that the calibration procedure results in somewhat increased estimates for prebomb surface ocean $\Delta^{14}C$ at high latitudes, decreased estimates for low latitudes, and approximately the same estimate for mid latitudes. The blue line is a loess fit to the values generated using GEOSECS surface ocean silicate concentrations and the function derived in B95 (equation (1)).

[39] The corrected potential alkalinity method clearly provides a better estimate of the prebomb surface ocean $\Delta^{14}C$ distribution than either the original potential alkalinity method or the silicate method. It must be stressed the B95 did not suggest that their silicate function (equation (1)) be used for surface ocean estimates. Rather, they approximated surface ocean values from the early measurements. This emphasis derives from the fact that silicate based surface ocean estimates are clearly too low for most of the ocean and that recent publications have tended to use this estimate simply because it could be readily calculated [e.g., *Tsunogai et al.*, 1995; *Peng et al.*, 1998; *Sonnerup et al.*, 1999; *Watanabe et al.*, 1999; *Mahadevan*, 2001]. Underestimation of the surface ocean prebomb $\Delta^{14}C$ will lead to an overestimation of the surface ocean bomb-produced $\Delta^{14}C$. In Figure 14, one low latitude ocean measurement (5°N, $\Delta^{14}C \sim -100‰$) is very anomalous relative to the coral data, the other ocean data, and the value predicted by the corrected Palk function. If real, this sample must have captured a particularly strong upwelling event. Given the measurement time and procedure, the value may not be good.

7. Bomb Radiocarbon Inventories

[40] Both the silicate and potential alkalinity methods are used to approximate the natural $\Delta^{14}C$ distribution in the water column. For the Palk method, equation (9) is used for the mixed layer and equation (3) for the rest of the bomb contaminated thermocline region. The difference between the measured $\Delta^{14}C$ and the predicted natural $\Delta^{14}C$ is the bomb radiocarbon. Figure 15 illustrates the technique (GEOSECS Station 429 at 48°S, 58°E in the Indian Ocean). The symbols indicate the measured $\Delta^{14}C$ (asterisks) and estimated natural $\Delta^{14}C$ using the silicate (solid triangle, B95) and potential alkalinity (circles) methods. The double hatched region indicates the bomb radiocarbon using the silicate method (6.4×10^9 atoms cm^{-2}). The Palk method adds the single-hatched region

Table 4. Summary Comparison of Results Using the Silicate and Potential Alkalinity Methods to Estimate Natural and Bomb Radiocarbon Values and Inventories

Station	Latitude	Longitude	B95 Surface Natural $\Delta^{14}C$ ‰	B95 Surface Bomb $\Delta^{14}C$ ‰	B95 Bomb Inventory 10^9 atom/cm^2	Palk Surface Natural $\Delta^{14}C$ ‰	Palk Surface Bomb $\Delta^{14}C$ ‰	Palk Bomb Inventory 10^9atom/cm^2
				Atlantic Ocean				
3	51.025	−43.017	−55	63	17.6	-	-	-
5	56.943	−42.558	−55	104	17.5	-	-	-
11	63.53	−35.228	−55	90	16.9	-	-	-
17	74.933	−1.120	−55	102	14.1	-	-	-
18	70.000	−0.008	−55	122	19.4	-	-	-
19	64.200	−5.568	−55	102	14.3	-	-	-
23	60.413	−18.617	−55	103	16.1	-	-	-
27	42.000	−42.033	−48	171	23.4	−42	165	19.1
29	35.975	−47.008	−45	195	25.2	−53	203	22.4
31	27.000	−53.533	−44	230	17.6	−50	236	19.7
33	21.000	−54.000	−50	215	12.0	-	-	14.1
37	12.028	−50.995	−59	192	6.6	-	-	7.3
40	3.945	−38.517	−68	176	5.2	−66	173	6.0
48	−4.000	−29.000	−66	149	3.7	−76	-	4.1
49	−7.933	−28.200	−61	155	4.7	−70	164	5.3
54	−15.053	−29.518	−51	162	7.4	−63	174	8.4
56	−21.008	−33.000	−41	179	9.6	−53	190	9.9
58	−27.000	−37.022	−41	189	10.5	−58	207	12.8
60	−32.967	−42.508	−41	174	12.7	−58	191	15.8
64	−39.058	−48.550	−59	151	7.9	-	-	9.4
67	−44.967	−51.058	−78	150	10.1	−70	140	13.4
68	−48.650	−45.985	−70	115	8.0	-	-	-
74	−55.008	−50.075	−86	89	3.7	-	-	-
76	−57.733	−66.133	−74	94	5.4	-	-	7.1
78	−61.050	−62.967	−100	81	2.8	-	-	1.7
79	−59.942	−45.033	-	-	-	-	-	-
82	−56.260	−24.918	−114	52	2.1	−129	67	1.8
89	−60.013	0.033	−125	82	2.3	−138	95	2.3
90	−56.427	4.510	-	-	-	−134	78	-
91	−49.570	11.467	−70	89	4.2	−128	147	6.9
92	−46.183	14.612	-	-	-	−105	168	-
93	−41.767	18.452	−68	158	10.6	-	-	8.4
103	−23.995	8.503	−41	115	7.4	−67	-	6.7
107	−12.000	2.000	−55	111	2.6	−71	131	2.7
109	−2.000	−4.500	-	-	-	-	-	-
111	2.008	−14.025	−70	130	3.2	−68	128	3.4
113	10.983	−20.517	−61	142	1.9	−75	53	1.0
114	21.175	−21.775	-	-	-	-	-	-
115	28.025	−26.000	−43	167	13.0	−52	175	12.1
117	30.675	−38.967	−41	180	18.8	-	-	12.5
120	33.267	−56.550	−43	171	21.0	−41	169	13.9
				Pacific Ocean				
201	34.175	−127.895	−50	239	8.9	−102	290	10.4
202	33.100	−139.572	−50	256	11.1	−75	281	12.4
204	31.378	−150.033	−50	228	9.9	−68	247	9.8
212	30.000	−159.842	-	-	-	-	-	3.5
213	30.967	−168.475	−50	237	11.1	-	-	10.2
214	32.025	−176.997	−50	195	11.9	−66	211	14.1
217	44.612	−176.835	−88	156	8.4	−114	-	10.4
218	50.445	−176.583	−86	149	7.1	-	-	3.2
219	53.105	−177.305	−102	116	7.4	−147	160	8.0
222	40.167	160.500	−72	156	7.8	−90	174	9.8
223	34.972	151.842	−50	213	16.3	−67	230	19.3
224	34.258	141.967	−50	182	15.8	−58	189	16.7
225	32.617	161.925	−50	200	14.9	−62	212	14.1
226	30.567	170.642	−50	210	11.8	−50	210	11.5
227	24.992	170.083	−50	235	12	-	-	5.1
229	12.883	173.467	−50	183	8.4	−77	208	8.2
231	14.108	−178.633	−50	195	9.1	-	-	5.8
235	16.758	−161.328	−50	195	7.6	−60	205	8.3
239	5.883	−172.013	−50	134	5.7	−86	165	5.9
241	4.562	179.002	−50	137	5.7	−83	171	7.2
246	0.000	179.000	−50	122	5.5	−97	169	9.4
251	−4.567	179.000	−50	135	6.2	−83	168	10.5

Table 4. (continued)

Station	Latitude	Longitude	B95 Surface Natural $\Delta^{14}C$ ‰	B95 Surface Bomb $\Delta^{14}C$ ‰	B95 Bomb Inventory 10^9 atom/cm^2	Palk Surface Natural $\Delta^{14}C$ ‰	Palk Surface Bomb $\Delta^{14}C$ ‰	Palk Bomb Inventory 10^9atom/cm^2
257	−10.175	−169.975	−50	152	7.7	−75	177	8.9
263	−16.697	−167.060	−50	187	9.9	−90	228	15.6
269	−23.963	−174.520	−50	174	12.3	-	-	7.6
282	−57.517	169.783	−73	116	6.9	−129	174	12.9
287	−69.300	−173.500	−125	48	1.6	−139	62	-
290	−58.017	−174.000	−71	87	5.0	-	-	8.9
293	−52.583	−178.033	−71	127	11.3	−84	140	16.4
296	−44.947	−166.658	−64	143	9.7	-	-	8.5
303	−38.380	−170.070	−58	167	11.7	−61	171	14.9
306	−32.833	−163.633	−53	192	9.4	−54	-	8.4
310	−26.958	−157.158	−50	209	11.3	-	-	8.2
317	−23.633	−127.153	−50	191	11.4	−76	217	12.0
320	−33.343	−128.402	−53	224	9.7	−76	247	13.5
322	−43.008	−129.947	−62	172	10.8	−86	196	16.2
324	−23.008	−146.075	−50	205	10.5	-	-	1.1
326	−14.053	−126.260	−50	95	7.7	−79	-	5.9
331	−4.633	−125.133	−50	91	3.6	−87	127	3.5
334	0.063	−124.567	−50	123	3.4	−80	153	-
337	4.847	−124.083	−50	111	3.2	−75	137	3.1
343	16.520	−122.992	−50	180	5.1	−78	-	1.2
347	28.512	−121.485	−50	244	12.3	-	-	-
				Mediterranean Sea				
404	35.597	17.252	−52	144	13.7	-	-	-
				Indian Ocean				
409	12.168	43.950	-	-	-	−53	125	4.2
413	13.363	53.267	−65	137	7.1	−48	106	3.0
416	19.758	64.617	−68	127	6.2	−48	122	2.5
417	12.970	64.478	−65	140	5.0	−57	132	4.4
418	6.185	64.420	−62	137	6.0	−52	147	3.5
419	3.95	56.802	−61	156	5.4	−67	160	5.2
420	−0.050	50.928	−59	152	5.4	−60	154	3.8
421	−6.152	50.910	−56	151	4.5	-	-	-
424	−12.305	53.688	−53	164	9.1	-	-	-
425	−17.300	55.850	-	-	-	−44	173	16.7
427	−27.068	56.967	−51	180	17.3	−47	146	18.0
428	−37.758	57.627	−68	166	17.5	−114	142	8.7
429	−47.667	57.860	−75	103	6.4	-	-	-
430	−59.983	60.975	−113	93	4.6	−132	65	0.9
431	−64.188	83.978	−115	48	1.7	-	-	1.0
432	−59.32	92.638	−130	76	3.5	−127	112	4.6
433	−53.013	103.025	−82	67	4.9	-	-	11.9
435	−39.952	109.970	−71	169	17.8	−50	191	15.9
436	−29.250	109.967	−54	194	16.8	−52	201	17.2
437	−24.475	104.928	−48	197	16.1	−48	186	13.2
438	−19.487	101.292	−50	187	13.4	-	-	4.6
439	−13.035	97.147	−53	183	8.9	-	-	2.5
440	−9.362	95.027	−55	159	4.6	−59	181	4.3
441	−5.027	91.778	−57	179	4.6	−62	182	3.7
442	−1.200	90.753	−59	178	4.6	−65	167	3.2
445	8.522	86.042	−63	165	4.1	-	-	-
446	12.525	84.510	−65	181	5.2	−88	204	4.2
447	4.995	79.952	−61	166	4.6	−72	177	3.4
448	0.017	80.053	−59	172	5.3	−63	176	4.3
449	−5.005	79.995	−57	171	4.7	−59	175	3.9
450	−10.008	79.985	−54	183	6.1	−59	188	5.0
451	−14.985	79.958	−52	179	11.9	−52	178	11.2
452	−20.093	79.983	−50	174	16.4	-	-	13.7
453	−23.000	74.017	−48	191	16.6	−49	192	15.9
454	−26.993	67.097	−51	185	17.9	−45	180	17.5

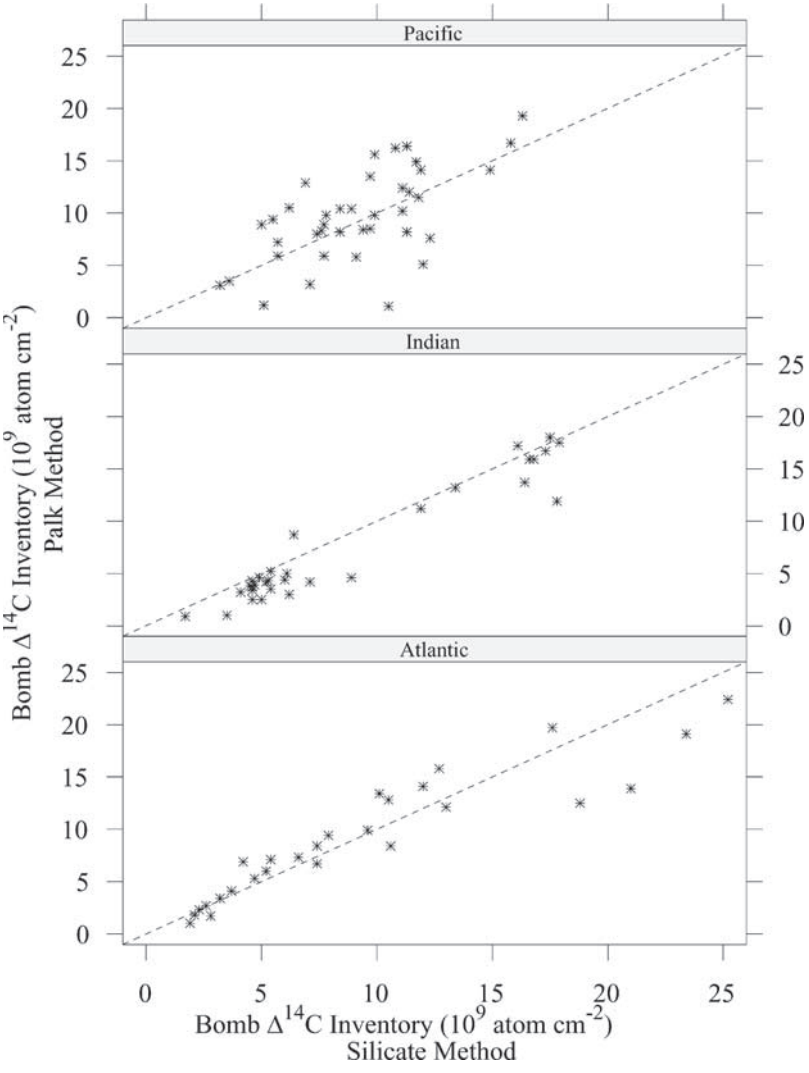

Figure 16. Bomb radiocarbon inventory comparison for the silicate (B95) and potential alkalinity (Palk) methods. Values are in 10^9 ^{14}C atoms cm^{-2}. The diagonal line in each subplot is the intercept = 0, slope = 1 ideal relationship.

(10.0×10^9 atoms cm^{-2}). To get an inventory, integration of the hatched region is carried down to the point where the measured and natural values are equal or, to the approximate point of zero tritium activity. Bomb radiocarbon estimates are converted from per mil units to atoms per mass prior to integration.

[41] The results from Figure 6 demonstrate that, on average, the Palk and silicate methods yield comparable estimates of natural Δ^{14}C for mid- and low-latitude waters. This does not imply that the methods yield comparable results for every (or for that matter, any) station. In some cases, the estimated natural and measured Δ^{14}C values do not converge. In that situation, one must decide how and where to terminate the integration, or to totally disregard such stations. Here, selection of the lower integration limit was taken as the shallowest depth where the bomb radiocarbon either approximated zero or went through a "low" concentration minimum. Stations where the integration limit was really unclear based on the bomb radiocarbon estimates were disregarded.

[42] Results using both the silicate and potential alkalinity methods are summarized in Table 4. The columns titled "B95..." reproduce results from Table 1 of B95. Those titled "Palk..." are from this work. Results from the two inventory columns of Table 4 are segregated by ocean and plotted against each other in Figure 16. The diagonal line in each panel indicates the 1:1 ideal relationship. The result is similar to that shown in Figure 6. The increase in scatter relative to Figure 6 reflects the additional error incurred due to integration.

8. Conclusions

[43] A new method based on the correlation of potential alkalinity and radiocarbon is presented which allows separation of bomb-produced and natural radiocarbon in open

ocean waters. The advantages are that the potential alkalinity method can be used for all open ocean waters and for estimates of prebomb surface ocean values. The primary disadvantage, relative to the B95 method, is that high quality alkalinity measurements are less common than high quality silicate measurements. For low- and mid-latitude waters, both methods give comparable results. For high latitude southern waters, the potential alkalinity method predicts lower natural $\Delta^{14}C$ and consequently higher bomb radiocarbon.

[44] Implications of the inventory difference between the silicate and Palk methods relative to air-sea gas fluxes, tritium distributions and anthropogenic CO_2 distribution and inventory were not addressed here. The WOCE radiocarbon and CO_2 results are rapidly becoming available and will be used for that study.

[45] **Acknowledgments.** This work was supported by National Science Foundation grants OCE-9617972, OCE-9618017 and OCE-9986310. Special thanks to J.R. Toggweiler for significant input during many discussions and to the two reviewers whose comments helped us to clarify the text.

References

Bien, G. S., N. W. Rakestraw, and H. E. Suess, Radiocarbon concentration in Pacific Ocean water, *Tellus*, *12*, 436–443, 1960.

Bien, G. S., N. W. Rakestraw, and H. E. Suess, Radiocarbon in the Pacific and Indian Oceans and its relation to deep water movements, *Limnol. Oceanogr.*, *10*(Suppl.), R25–R37, 1965.

Brewer, P. G., and J. C. Goldman, Alkalinity changes generated by phytoplankton growth, *Limnol. Oceanogr.*, *21*, 108–117, 1976.

Broecker, W. S., R. Gerard, M. Ewing, and B. H. Heezen, Natural radiocarbon in the Atlantic Ocean, *J. Geophys. Res.*, *65*, 2903–2931, 1960.

Broecker, W. S., T.-H. Peng, G. Östlund, and M. Stuiver, The distribution of bomb radiocarbon in the ocean, *J. Geophys. Res.*, *90*, 6953–6970, 1985.

Broecker, W. S., S. Sutherland, W. Smethie, T.-H. Peng, and G. Östlund, Oceanic radiocarbon: Separation of the natural and bomb components, *Global Biogeochem. Cycles*, *9*(2), 263–288, 1995.

Craig, H., W. Broecker, and D. Spencer, *Sections and Profiles, 1973–1974, GEOSECS Pacific Expedition*, vol. 4, U. S. Gov. Print. Off., Washington, D. C., 1981.

Druffel, E. M., Radiocarbon in annual coral rings from the eastern tropical Pacific, *Geophys. Res. Lett.*, *8*, 59–62, 1981.

Druffel, E. R. M., Bomb radiocarbon in the Pacific: Annual and seasonal time scale variations, *J. Mar. Res.*, *45*, 667–698, 1987.

Druffel, E. R. M., Pacific bomb radiocarbon coral data, *Data Contrib. Ser. 1995-011*, World Data Cent. A for Paleoclimatol., Boulder, Colo., 1995.

Fiadiero, M. E., Three-dimensional modeling of tracers in the deep Pacific Ocean II: Radiocarbon and circulation, *J. Mar. Res.*, *40*, 537–550, 1982.

Fonselius, S., and G. Östlund, Natural radiocarbon measurements on surface water from the North Atlantic and the Arctic Sea, *Tellus*, *11*, 77–82, 1959.

George, M. D., M. D. Kumar, S. W. A. Naqvi, S. Banerjee, P. V. Narvekar, S. N. de Sousa, and D. A. Jayakumar, A study of the carbon dioxide system in the northern Indian Ocean during pre-monsoon, *Mar. Chem.*, *47*, 243–254, 1994.

Guilderson, T. P., and D. Schrag, Urvina Bay (Galapagos) coral radiocarbon data, World Data Cent. A for Paleoclimatol., *Data Contrib. Ser. 1999-051*, Boulder, Colo., 1999.

Guilderson, T. P., et al., Nauru Island coral radiocarbon data, World Data Cent. A for Paleoclimatol., *Data Contrib. Ser. 1999-043*, Boulder, Colo., 1999.

Honjo, S., J. Dymond, W. Prell, and V. Ittekkot, Monsoon-controlled export fluxes to the interior of the Arabian Sea, *Deep Sea Res., Part II*, *46*, 1859–1902, 1999.

Ittekkot, V., R. R. Nair, S. Honjo, V. Ramaswamy, M. Bartsch, S. Manganini, and B. N. Desai, Enhanced particle fluxes in Bay of Bengal induced by injection of fresh water, *Nature*, *351*, 385–387, 1991.

Jenkins, W. J., Tritium and 3He in the Sargasso Sea, *J. Mar. Res.*, *38*, 533–569, 1980.

Joyce, T., and C. Corry (Eds.), Requirements for WOCE Hydrographic Programme data reporting, *WHPO Pub. 90-1 Rev. 2*, 145 pp., WOCE Hydrogr. Program Off., La Jolla, Calif., 1994a.

Joyce, T., and C. Corry (Eds), 1994 WOCE Operations Manual, vol. 3, The Observational Programme, sect. 3.1, WOCE Hydrographic Programme, part 3.1.3, WHP Operations and Methods, *WHP Off. Rep. WHPO 91-1*, Woce Hydrographic Program Office, La Jolla, Calif., 1994b.

Lamb, M. F., et al., Consistency and synthesis of Pacific Ocean CO_2 survey data, *Deep Sea Res., Part II*, *49*(1–3), 21–58, 2002.

Leboucher, V., J. Orr, P. Jean-Baptiste, M. Arnold, P. Monfray, N. Tisnerat-Laborde, A. Poisson, and J.-C. Duplessy, Oceanic radiocarbon between Antarctica and South Africa along WOCE section I6 at 30°E, *Radiocarbon*, *41*(1), 51–73, 1999.

Levin, I., R. Graul, and N. B. A. Trivett, Long-term observations of atmospheric CO_2 and carbon isotopes at continental sites in Germany, *Tellus, Ser. B*, *47*, 23–34, 1995.

Mahadevan, A., An analysis of bomb radiocarbon trends in the Pacific, *Mar. Chem.*, *73*, 273–290, 2001.

Manning, M. R., and W. H. Melhuish, Atmospheric $\Delta^{14}C$ record from Wellington, in *Trends: A Compendium of Data on Global Change*, Carbon Dioxide Inf. Anal. Cent., Oak Ridge Natl. Lab., U. S. Dep. Of Energy, Oak Ridge, Tenn., 1994.

Nair, R. R., V. Ittekkot, S. J. Manganini, V. Ramaswamy, B. Haake, E.T. Degens, B.N. Desai, and S. Honjo, Increased particle flux to the deep ocean related to monsoons, *Nature*, *338*, 749–751, 1989.

Östlund, H. G., H. Craig, W. S. Broecker, and D. Spencer, *GEOSECS Atlantic, Pacific, and Indian Ocean Expeditions*, vol. 7, *Shorebased Data and Graphics*, U. S. Gov. Printing Off., Washington, D. C., 1987.

Peng, T.-H., R. M. Key, and H. G. Östlund, Temporal variations of bomb radiocarbon inventory in the Pacific Ocean, *Mar. Chem.*, *60*, 3–14, 1998.

Rafter, T. A., Carbon-14 variations in nature, 3, ^{14}C measurements in the South Pacific and Antarctic Oceans, *New Zealand J. Sci.*, *11*(4), 551–589, 1968.

Sabine, C. L., R. M. Key, K. Johnson, F. J. Millero, J. Sarmiento, D. Wallace, and C. Winn, Anthropogenic CO_2 inventory of the Indian Ocean, *Global Biogeochem. Cycles*, *13*(1), 179–198, 1999.

Sabine, C. L., R. M. Key, R. A. Feely, and D. Greeley, Inorganic carbon in the Indian Ocean: Distribution and dissolution processes, *Global Biogeochem. Cycles*, *16*(4), 1067, 10.1029/2002GB001869, in press, 2002.

Sonnerup, R. E., P. D. Quay, and J. L. Bullister, Thermocline ventilation and oxygen utilization rates in the subtropical North Pacific based on CFC distributions during WOCE, *Deep Sea Res., Part I*, *46*, 777–805, 1999.

Stuiver, M., P. J. Reimer, and T. F. Braziunas, High-precision radiocarbon age calibration for terrestrial and marine samples, *Radiocarbon*, *40*, 1127–1151, 1998.

Toggweiler, J. R., K. Dixon, and W. S. Broecker, The Peru upwelling and the ventilation of the South Pacific thermocline, *J. Geophys. Res.*, *96*(C11), 20,467–20,497, 1991.

Tsunogai, S., S. Watanabe, M. Honda, and T. Aramaki, North Pacific Intermediate Water studied chiefly with radiocarbon, *J. Oceanogr.*, *51*, 519–536, 1995.

Watanabe, Y. W., T. Ono, K. Harada, and M. Fukasawa, A preliminary study of oceanic bomb radiocarbon inventory in the North Pacific during the last two decades, *J. Oceanogr.*, *55*, 705–716, 1999.

R. M. Key, Atmospheric and Oceanic Sciences Program, Sayre Hall, Princeton University, Princeton, N. J. 08544, USA. (key@princeton.edu)

S. I. Rubin, Department of Earth and Atmospheric Sciences, Georgia Institute of Technology, Ford ES&T Building, 311 Ferst Drive, Atlanta, GA 30332, USA. (srubin@eas.gatech.edu)